Correlation-function spectroscopy of inelastic lifetime in heavily doped GaAs heterostructures

J. Könemann,[1] P. König,[1] T. Schmidt,[1] E. McCann,[2] Vladimir I. Fal'ko,[2] and R. J. Haug[1]
[1]*Institut für Festkörperphysik, Universität Hannover, Appelstrasse 2, 30167 Hannover, Germany*
[2]*Department of Physics, Lancaster University, Lancaster, LA1 4YB, United Kingdom*
(Received 11 April 2001; published 19 September 2001)

Measurements of resonant tunneling through a localized impurity state are used to probe fluctuations in the local density of states of heavily doped GaAs. The measured differential conductance is analyzed in terms of correlation functions with respect to voltage. A qualitative picture based on the scaling theory of Thouless is developed to relate the observed fluctuations to the statistics of single-particle wave functions. In a quantitative theory correlation functions are calculated. By comparing the experimental and theoretical correlation functions, the effective dimensionality of the emitter is analyzed and the dependence of the inelastic lifetime on energy is extracted.

DOI: 10.1103/PhysRevB.64.155314 PACS number(s): 73.23.−b, 72.20.My, 85.30.Mn

I. INTRODUCTION

The observation of impurity-assisted tunneling in vertical transport experiments on double-barrier semiconductor heterostructures[1–5] led to the possibility of using the resonant impurity level as a local probe of electronic states of electrodes prepared from heavily doped degenerate semiconductors. A number of experiments in strongly asymmetric double-barrier structures have measured directly the local density of states (LDOS) of an electrode as a function of excitation energy E from the Fermi level,[5–10] those with the highest spectral resolution reporting features including the Zeeman splitting of single-particle levels in a disordered emitter.[9]

The idea of such experiments is illustrated by the sketch in Fig. 1. Electrons tunnel from a heavily doped disordered emitter through the energetically lowest level of the quantum well sandwiched between the double barriers. This energetically lowest level of the quantum well serves as the spectrometer S. At zero bias, the energy of this impurity level, E_S, does not coincide with the chemical potential μ in the emitter. It comes to resonance only after the bias voltage reaches a threshold value $V_S(E_S)$. Typical current-voltage $I(V)$ characteristics of such a device can be divided into three intervals:[2–5,11] one interval below the threshold, where $I \approx 0$; the threshold regime $V \approx V_S(E_S)$, where $I(V)$ undergoes a jump when the resonant level crosses the Fermi level μ in the emitter, and the interval of a plateau, $V_S(E_S) < V < V_1(E_1)$, where the current remains nearly constant. The latter interval lasts until the next impurity level E_1 is lowered enough to contribute to the transport and it is ideal for studying the image of the LDOS in the emitting reservoir,[5,12] since any further variation of the current as a function of bias voltage, $I(V)$ is dominated by the energy dependence of the tunneling density of states in the emitter, $I(V) \propto \nu(E)$. A convenient way to look at such $I(V)$ characteristics is to plot the differential conductance $G(V) = dI/dV \propto d\nu/dE$, in which the image of variation in LDOS is more pronounced.

In a disordered medium, the energy dependence of the LDOS studied at a certain point of a sample reveals an irregular fine structure,[13] $\nu(E) = \nu_0 + \delta\nu(E)$, which arises from quantum interference of elastically scattered quasiparticles[14] diffusing coherently within a length scale related to their lifetime at a particular energy. Since the Aharonov-Bohm phase accumulated by a diffusing particle in a magnetic field changes the interference pattern, such a fine structure, $\delta\nu(E)$, depends randomly on a magnetic field B. In tunneling experiments, the interfering quasiparticle is, in fact, a ''hole'' in the Fermi sea left behind by the tunneling of an electron out of the emitter with $E < \mu$. Being in a nonequilibrium state, such a hole ''floats up'' towards the Fermi level, due to inelastic collisions between electrons, so that it can be characterized by a finite lifetime equivalent to a broadening of emitter states.[11] The broadening of emitter states suppresses the finest features in the LDOS fluctuations, and, therefore, it strongly affects the amplitude and correlation parameters of fluctuations of the differential conductance[12] of a given resonant tunneling device, $\delta G(V) = G(V) - \langle G \rangle$. A particularly convenient situation to study fluctuations is realized in devices where the mean value of the density of states in the emitter and also the transmission through the barriers varies much slower than fine fluctuations in LDOS, so that within the narrow energy interval below the Fermi energy of the emitter $\langle G \rangle$ is negligible and $\delta G(V) \approx G(V)$.

Recently, we reported[10] an experiment where the speeding up of the quasiparticle relaxation upon the increase of the energetic distance to the Fermi level (equal to the excitation energy of the Fermi sea holes) was observed via the decline in the variance of differential conductance fluctuations at higher bias voltages, $\langle (\delta G)^2 \rangle$. In the present publication, we study the correlation function, $K(V)$, of a random differential conductance pattern worked out for different bias voltage intervals. To make this analysis sound, the differential conductance of a resonant tunneling structure has been measured for a dense grid of magnetic field values, which has largely increased the statistical ensemble of data used in the evaluation of the correlation function $K(\Delta V)$ of a random pattern $\delta G(V,B)$,

$$K(\Delta V) = \frac{\langle \delta G(V+\Delta V,B)\, \delta G(V,B) \rangle_B}{\langle (\delta G)^2 \rangle_B}, \qquad (1)$$

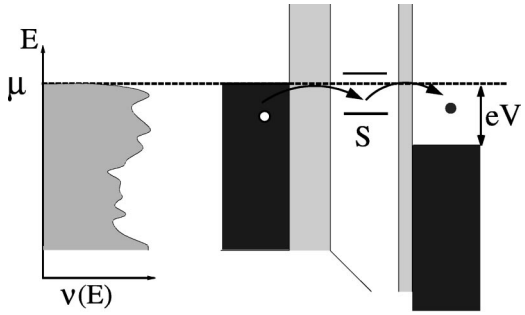

FIG. 1. Sketch of the resonant tunneling spectroscopy of the LDOS using an impurity state in a double-barrier structure. Electrons tunnel from a heavily doped disordered emitter through the energetically lowest level S of the quantum well sandwiched between the double barriers, so that S serves as a spectrometer of the density of states $\nu(E)$ of the emitter.

and has allowed us to compare details of its shape to the results of a theoretical analysis. The latter effort has enabled us to notice some geometrical features of the structure used in this experiment (produced in a particular growth process), which would be difficult to detect otherwise.

The material presented in this paper is organized as follows. In Sec. II, the experimental setup, parameters, and design of the structures that we used, and the raw data of $G(V)$ characteristics are discussed. In order to characterize the spectral resolution of the spectrometer, we analyze in Sec. II the form of $\langle G(V)\rangle_B$ averaged over many runs taken at different values of applied magnetic field. A detailed quantitative analysis of fluctuations and their correlation functions is presented in Sec. III, in comparison to the results of a theory presented in two Appendixes. The end of Sec. III is devoted to the discussion of the energy dependence of the quasiparticle relaxation rate extracted from this analysis, from the point of view of the Aronov-Altshuler theory of electron-electron interaction in disordered metals.[15,16] Appendix A completes the text with a qualitative estimation of the variance of the differential conductance fluctuations [17–21] based upon the theory of statistical and correlation properties of chaotic wave functions in disordered media[22–24] using an approach similar to the Thouless scaling theory.[25] The quantitative analysis of the variance and correlation properties of a pattern of $\delta G(V)$, including the dimensional crossover, is presented in Appendix B.

II. SAMPLES AND EXPERIMENTAL RESULTS

The experiment was performed using an asymmetric double-barrier heterostructure that was grown by molecular-beam epitaxy on an n^+-type GaAs substrate. Directly on top of the substrate the layer sequence for the resonant tunneling diode was grown as illustrated in Fig. 2. The growth started with a 300 nm thick GaAs layer doped with Si to 4.0×10^{17} cm^{-3}. This emitter layer is followed by a very thin spacer layer of 7 nm undoped GaAs. The actual resonant tunneling structure consists of a 10 nm wide GaAs quantum well sandwiched between two $Al_{0.3}Ga_{0.7}As$ barriers of 5 and 8 nm width (top and bottom barrier). The collector of the

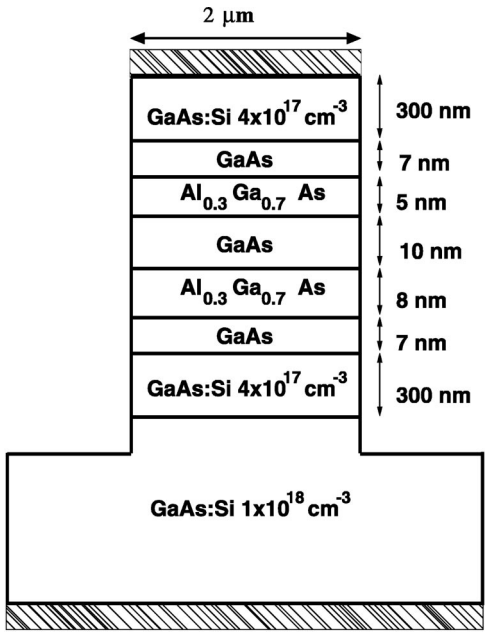

FIG. 2. Layer structure of the double-barrier heterostructure.

structure is formed by a second spacer layer of 7 nm undoped GaAs and a 300 nm thick layer of GaAs doped with Si to 4.0×10^{17} cm^{-3}.

The barrier structure is highly asymmetric, and the transparency of the thick emitter barrier is much lower than that of the collector barrier, which means that the value of the tunneling current is dominated by the low transmission of the emitter barrier. Due to the thin spacer layer the nominally undoped quantum well contains a small number of residual impurities. The energetically lowest impurity state will be used as a local spectrometer of the emitter states.

In order to limit the number of residual impurities in the quantum well, pillars with small areas were fabricated from this heterostructure.[26] By employing electron-beam lithography, evaporation, and lift-off, AuGe/Ni layers were deposited on the top of the wafer. This metallization served both as an Ohmic contact and as an etch mask for the following reactive ion etching (RIE) step. A AuGe/Ni coating was also evaporated onto the substrate side of the wafer to form the back Ohmic contact. Free-standing pillars with diameters in the μm and sub-μm range and a typical height of several hundred nm were etched using RIE. Then, large-area Cr/Ag/Au bond pads could be prepared on top of the pillars by planarizing the pillars with an insulating polyimide layer. The tunneling current was measured with a dc technique in a dilution refrigerator at 20 mK base temperature. For our analysis the differential conductance $G(V)$ was numerically calculated from the measured current values. A typical $G(V)$ trace is shown in Fig. 3. At zero bias, S lies above the Fermi level in the emitter and is not available for resonant transport, resulting in $G=0$. At $V_S=9.8$ mV, the spectrometer crosses the Fermi level and the current jumps abruptly from zero to a finite value, resulting in a sharp peak in the derivative $G\propto d\nu/d\epsilon$. For larger bias voltages a reproducible oscillatory fine structure can be seen, which we attribute as the result of LDOS fluctuations in the contact regions. This fine

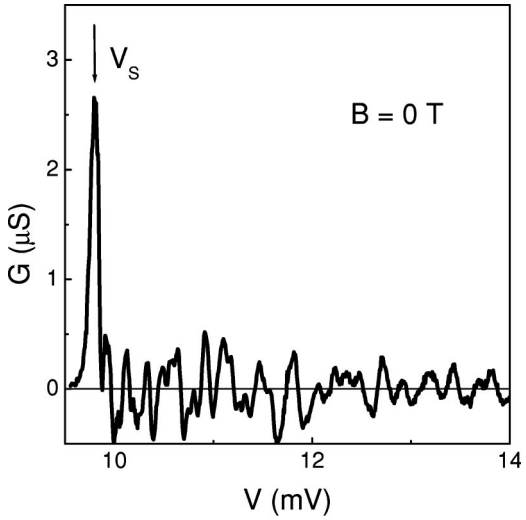

FIG. 3. Image of LDOS fluctuations: Typical plot of the differential conductance G versus bias voltage V at $B=0$ T and a base temperature of $T=20$ mK.

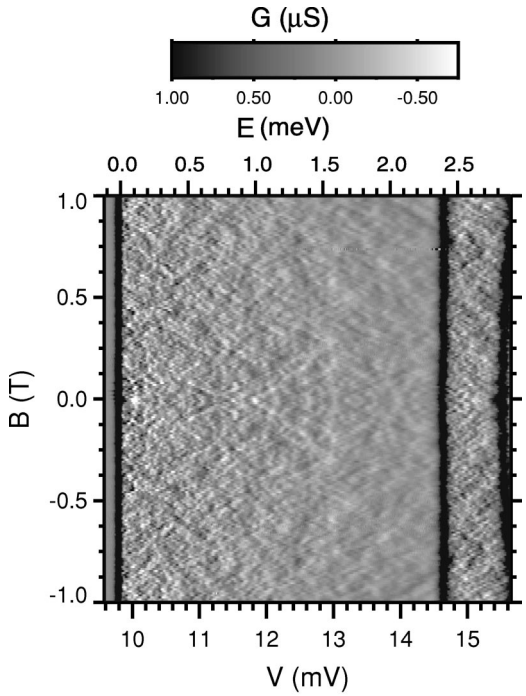

FIG. 4. Contour plot of the differential conductance G as a function of bias voltage V (step 7 μV) and magnetic field $B\|I$ (step 10 mT) for $T=20$ mK. The excitation energy E on the top scale is converted from the bias voltage V; see text.

structure is formed by electrons that tunnel from below the emitter Fermi level through the lowest discrete state S in the quantum well. Since the emitter barrier is much stronger than the collector barrier, the value of the current step is mainly determined by the tunneling rate $\Gamma_l/\hbar$ through the thick barrier on the emitter side. Due to this large barrier asymmetry the $G(V)$ curve at voltages $V>9.8$ mV represents the energy dependence only of the LDOS $d\nu/d\epsilon$ in the emitter contact. So the fine structure represents an image of emitter contact LDOS fluctuations scanned by the impurity-related level in the quantum well.[5]

The quantum interference interpretation of the observed fine structure is supported by the observed effect of an applied magnetic field. The oscillatory form of $G(V)$ randomly changes upon variation of a magnetic field, at the scale $\Delta B<30$ mT. Figure 4 shows a gray-scale image of the differential conductance measured as a function of both bias voltage and a magnetic field within the interval of fields -1 T $<B<1$ T, where the Landau quantization of states in the emitter is completely suppressed by disorder. This diagram is symmetric with respect to magnetic field inversion, as it should be for a two-terminal measurement. The use of magnetic field enables us to get a sound amount of data for the following statistical analysis of fluctuations.

The onset of resonant tunneling through the lowest-lying impurity state S appears in Fig. 4 as a black line at a voltage of 9.8 mV (parallel to the B axis). The second black line at a bias voltage of 14.6 mV appears when the next, higher-lying impurity state crosses the Fermi energy in the emitter. For voltages ranging from 9.8 mV up to 14.6 mV, the measured tunneling current results only from tunneling through the lowest-lying impurity state S. This state is used as a local spectrometer to scan the LDOS below the Fermi level in the emitter. Voltage and energy scales are related via $E=\alpha e(V-V_S)$ where the prefactor $\alpha=0.5$ accounts for the fact that only part of the voltage drops between the emitter and spectrometer.[1,2,4] Therefore, the plot in Fig. 4 covers an energy range of quasiparticle excitations of about $0\leqslant E\leqslant 2.4$ meV, which is indicated by an alternative scale for the horizontal axis on the upper side of this figure. The amplitude of $G(V)$ fluctuations decreases (fine structure is suppressed) with increasing bias voltage in the range 9.8 mV $<V<14.6$ mV (interval between two peaks). At the same time, the characteristic voltage scale dominating the fine structure increases, which is interpreted below to be the result of the inelastic broadening of quasiparticle states in the emitter. Note that although oscillations at larger energy scales are also present in $I(V)\propto\nu(E)$, their contribution to $G(V)$ is suppressed due to the differentiation. For a broad spectrometer both the amplitude and correlation voltage of fluctuations would be the same over the entire range of $V_S\leqslant V\leqslant V_1$. For a narrow spectrometer, as studied in the present work, inelastic broadening of states in the bulk exceeds the spectrometer width upon increasing the excitation energy of a quasihole left in the emitter. Then, this inelastic broadening affects the parameter of the fluctuation pattern. Note that the observed fluctuations become sharp and large again after the second impurity level begins to contribute to the current at $V>14.6$ mV. This is because tunneling through the second impurity state involves states close to the Fermi energy that have negligible inelastic broadening. In the following, we shall focus on the tunneling through the lowest-lying impurity state, i.e. on the interval of bias voltages smaller than $V<14.6$ mV.

In Fig. 5 the differential conductance is shown after averaging the raw data $G(V,B)$ over the interval of magnetic field specified above. This averaging increases the contrast between the main peak corresponding to the spectrometer S

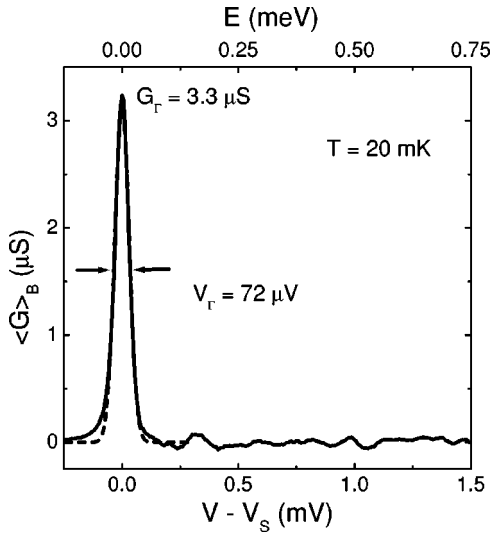

FIG. 5. The averaged differential conductance $\langle G(B)\rangle_B$ of the device obtained as described in the text.

crossing the emitter Fermi level and $\langle G(V)\rangle_B$ at larger bias voltages, where a random contribution from LDOS fluctuations is strongly suppressed. The fluctuations are suppressed by a statistical weight of $\sqrt{N}$, where N is the number of uncorrelated $G(V)$ traces taken at various magnetic fields. The plot in Fig. 5 can be used to extract the nominal spectrometer width, Γ. The emitter barrier in the device we study is thicker than the collector barrier, so that the broadening of the resonant level is dominated by electron escape from it to the collector, $\Gamma=\Gamma_r+\Gamma_l\approx\Gamma_r$, whereas the value of the current step is mainly determined by the tunneling rate $\Gamma_l/\hbar$ through the thick barrier on the emitter side. The averaged $\langle G(V)\rangle_B$ characteristics at the threshold can be parametrized[27–29] by the height of the conductance peak at the threshold voltage V_S and by its width V_Γ at the half-maximum, which is given by[30]

$$V_\Gamma\approx\Gamma/(e\alpha). \tag{2}$$

Below, we use $\Gamma=36$ μeV taken directly from Fig. 3.

III. STATISTICAL CHARACTERISTICS OF THE DIFFERENTIAL CONDUCTANCE FLUCTUATION PATTERN

In this section, we analyze correlation properties of the measured differential conductance pattern, aiming to extract from this the value and the form of the energy dependence of the decay rate for quasiparticles. The relevance of the correlation function of the fluctuation pattern for such an analysis arises because the autocorrelation function of fluctuations reflects the typical scale of their energy dependence (which is equivalent information to that in the power spectrum of frequencies of oscillations). To start with, the pattern of $\delta G(V)$ is random and it is related to the derivative of the LDOS with respect to energy, where the contribution from features at the finest energy scale is enhanced by differentiation. Therefore, the correlation function $K(\Delta V)=\langle\delta G(V+\Delta V,B)\,\delta G(V,B)\rangle/\langle\delta G^2\rangle$ carries information about the finest resolution of quantum states in the emitter. On the one hand, due to the finite spectrometer width, Γ, fine structure in the LDOS at energy scales smaller than Γ is smeared by the spectrometer, so that in the measurements reported above it cannot be resolved. On the other hand, the finest energy scale of LDOS fluctuations is intrinsically limited by inelastic broadening of quasiparticle states in the emitter, $\hbar\gamma$. As a result, the typical value of bias voltage, at which the differential conductance varies randomly, is determined by the sum of the above two,

$$V_c=\frac{1}{\alpha}[\Gamma+\hbar\gamma]=E_c/\alpha, \tag{3}$$

where the spectrometer width Γ is the same for the entire interval of energies of the quasihole in the emitter (left behind by the tunneling process) that we are able to study using one impurity state, whereas the inelastic broadening, $\hbar\gamma(E)$, is dependent on the excitation energy and varies across the studied bias voltage interval. The same combination of energetic parameters also determines the variance of the differential conductance fluctuations, $\langle\delta G^2\rangle$, which will be discussed in Sec. II B.

A. Correlation function of fluctuations

The experimental determination of the correlation function, K, consists of the evaluation of the variance $\langle\delta G^2\rangle_B$ and then the autocorrelation function of the measured differential conductance fluctuations pattern,

$$K(\Delta V)=\langle\delta G(V+\Delta V,B)\,\delta G(V,B)\rangle_B/\langle\delta G^2\rangle_B,$$

by means of averaging over different magnetic field points within the interval $0\ \mathrm{T}<B<1\ \mathrm{T}$. Then, the obtained correlation function is additionally averaged over a narrow interval of bias voltage, not more than 2–3 times broader than the width of the autocorrelation function determined after the first step. This procedure allows improved statistics and it slightly reduces variations in the form of the correlation function. Note that the finite amount of data used in this analysis still leaves space for statistical errors, so that the evaluated correlation function may be treated seriously only within an interval equal to 3 times its width at the half maximum.

The typical result we get for such a correlation function is shown in Fig. 6 for two values of bias voltage: one at the beginning of the studied interval, at $V=10.2$ mV, and the other at its end, at $V=13.8$ mV. These correlation functions have a very different width, which we attribute to an increase of inelastic broadening of states of quasiholes in the emitter upon the increase of their excitation energy, such that it becomes even larger than the spectrometer width, Γ. Therefore, the comparison of correlation parameters of $K(\Delta V)$ can be used for determining directly the value of the inelastic relaxation rate of quasiparticles in the emitter as a function of their excitation energy.

To obtain an absolute value of the inelastic broadening from such a comparison, one has to make a certain fit and, therefore, to use a certain form of the correlation function

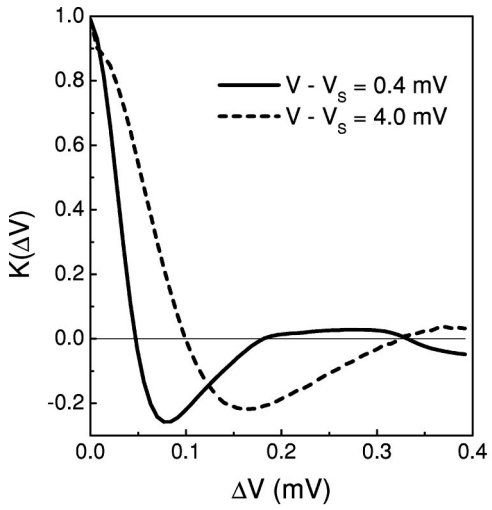

FIG. 6. Experimental correlation functions, taken at the beginning (solid, $V=10.2$ mV) and the end (dashed, $V=13.8$ mV) of the accessible voltage range.

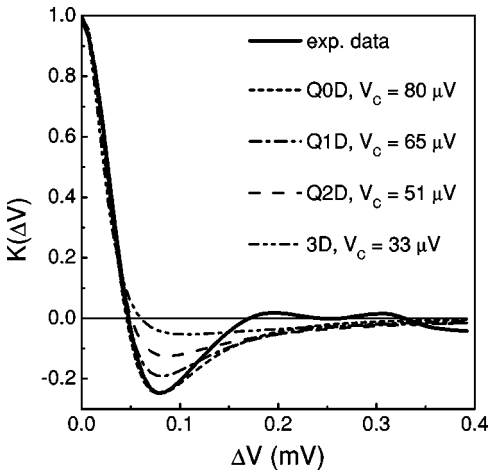

FIG. 7. The correlation function at the beginning of the accessible voltage range. The solid line is the experimental correlation function at $V=9.8$ mV and the other lines are fits based upon different assumptions about geometry.

$K(\Delta V)$. Theoretical analysis of the correlation function of differential conductance fluctuations in Ref. 12 has shown that its form and therefore the value of the correlation voltage extracted from the fit depend on the effective dimensionality of the diffusive emitter, that is, on its geometry. In particular, for a quasi-zero-dimensional (Q0D) emitter (diffusive pillar) and a quasi-2D film we have calculated

$$K_0(\Delta V)=\frac{1-3(\Delta V/V_c)^2}{[1+(\Delta V/V_c)^2]^3}, \tag{4}$$

$$K_2(\Delta V)=\frac{1-(\Delta V/V_c)^2}{[1+(\Delta V/V_c)^2]^2}.$$

For a quasi-1D wire and 3D bulk, these are, respectively,

$$K_1(\Delta V)=\frac{(4-2Y-Y^2)\sqrt{1+Y}}{\sqrt{2}Y^5},$$

$$K_3(\Delta V)=\frac{(2-Y)\sqrt{1+Y)}}{\sqrt{2}Y^3}, \tag{5}$$

$$Y=\sqrt{1+(\Delta V/V_c)^2}.$$

All these correlation functions were obtained in the unitary symmetry class limit for fluctuations.

In Fig. 7, all four are compared to the experimentally determined correlation function for the smallest bias voltage interval, i.e., for $V=9.8$ mV. Theoretical curves shown in this plot for various models of an emitter can be characterized by the depth of a negative anticorrelation overshoot in K, which is the most pronounced in the quasi-0D case. For each theoretical curve, the fit to the data is made using a single parameter, V_c, and the best agreement between the theory and experimental data is achieved for the quasi-0D model of the emitter.

The suggestion that the emitting electrode in the studied structure has the form of a box, rather than the form of a wire, which would be a natural assumption based upon the shape of the lithographically processed material in Fig. 2, needs an explanation. The point is that the emitter side of this device has been produced by overgrowing, heavily doped GaAs:Si substrate (10^{18} cm^{-3} of Si) with a 300 nm buffer layer of GaAs:Si, 4×10^{17} cm^{-3}. It is known that the interface between the substrate and the first grown layer is not as perfect as the interfaces produced during the molecular beam epitaxy (MBE) growth process. It is expected that at the interface between the substrate and the first layer a higher density of background impurities are incorporated and also that the dislocation density will be higher than that in the rest of the structure. The predominant background impurities will be carbon impurities, which act as acceptors in GaAs and compensate the Si-donor doping. Due to this compensation this interface could be poorly conducting. Although poor conduction through this interface does not affect the observable resistance value of the device and no other measurement performed on structures from the same series had enough sensitivity to indicate its presence, the LDOS fluctuation measurements appear to be sensitive enough to illuminate its existence.

For each given geometrical shape of the emitter (for this sample, a L-thick disk with a radius R), the effective dimensionality reflected by the shape of the correlation function in Eq. (4) also depends on the ratio between the diffusion length,

$$L_c=\sqrt{\frac{\hbar D}{\Gamma+\hbar\gamma}} \tag{6}$$

and geometrical sizes, L and R. The diffusion length in Eq. (6) characterizes the volume of a disordered system that is effectively tested by a coherently diffusing particle within the time scale taken before it either escapes from the emitting electrode to the collector via the resonant impurity S or re-

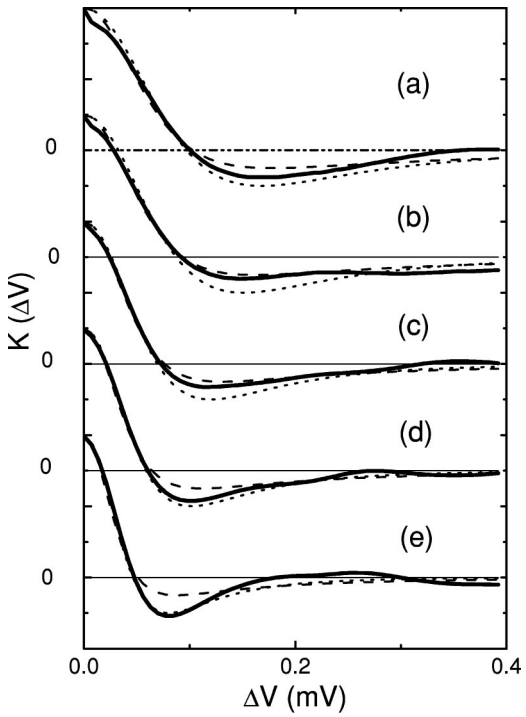

FIG. 8. The evolution of the correlation function from the beginning (bottom) to the end (top) of the accessible voltage range showing the experimental correlation function (solid) and fits for the quasi-0D (dotted) and quasi-2D model (dashed) for five voltages: (a) $V=13.8$ mV, (b) $V=13.0$ mV, (c) $V=12.2$ mV, (d) $V=11.4$ mV, and (e) $V=10.6$ mV.

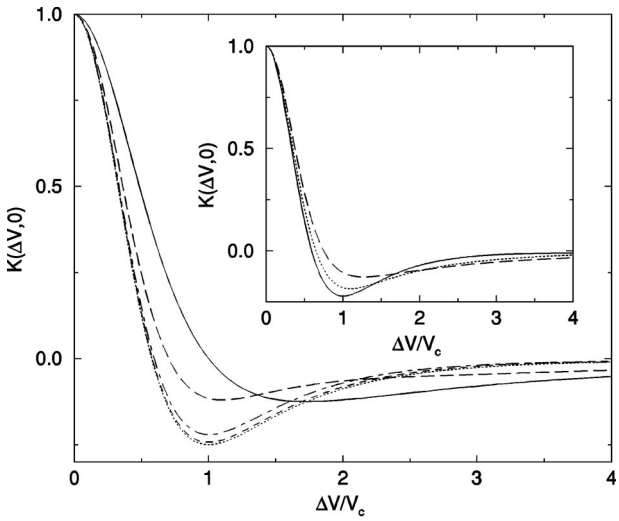

FIG. 9. Theoretical form of the correlation function $K(\Delta V)$ as a function of $\Delta V/V_c$ with the resonant impurity at the center of the disk $\rho/R=0$. Long dashed line is numerical result for $L_c/R=1.0$, dot-dashed line for $L_c/R=1.5$, and short dashed line for $L_c/R=2.0$. Solid and dotted lines are the analytic results in Eq. (4) for Q0D and Q2D geometry. Inset is $K(\Delta V,0)$ as a function of $\Delta V/V_c$ for $L_c/R=1.5$ and different impurity positions. Solid line is $\rho/R=0$, dotted line is $\rho/R=0.5$, and long dashed line is $\rho/R=1.0$.

laxes inelastically into states at different energies. When the latter length scale is the largest, $L_c \gg L,R$, the correlation function of fluctuations has the quasi-0D form. When $R>L_c>L$, the finite radius of a pillar would not matter, and the correlation function would have the quasi-2D form. Similarly, $L>L_c>R$ would correspond to the quasi-1D result in Eq. (4). Finally, one would have to treat the regime of $R,L \gg L_c$ as the three-dimensional one.

The value of the correlation voltage extracted from the fit of the experimental data in Fig. 7 using the quasi-0D model, $V_c=80$ μV is very close to the width of the main resonance peak in Fig. 5 determined by the intrinsic spectrometer width, $V_\Gamma=72$ μV. Comparison of V_Γ with other values of V_c obtained from fits of experimental $K(V)$ using other dimensionality assumptions ($V_c=65$ μV, 51 μV, and 33 μV for the Q1D, Q2D, and 3D models, respectively) gives an additional argument in favor of the view that we deal here with a quasi-0D emitter. At the same time, the relevant diffusion length L_c calculated as $L_c=\sqrt{D\hbar/E_c} \approx \sqrt{D\hbar/\Gamma}$ is longer than both the sample diameter and the width of the buffer layer, which would be consistent with an assumption that the interface is an obstacle for electron escape to the substrate.

Since the length scale L_c in Eq. (6) shortens, due to faster inelastic relaxation as the quasiparticle excitation energy increases, the effective dimensionality of the system may vary across the bias voltage interval we study. Since the sample used here has $R>L$, a crossover may take place between the quasi-0D and quasi-2D form of the correlation function that should be used for fitting the data in the broader voltage interval. One can find indications of such a crossover in the series of correlation functions shown in Fig. 8.

Traces of crossover behavior in Fig. 8 require one to make a detailed theoretical analysis of the intermediate regime $L_c \approx R$, since our final goal is to obtain quantitative information about the quasiparticle lifetime, as a function of quasiparticle energy in the entire energy interval assessed in the reported measurement. Details of a calculation of correlation functions in the crossover regime are presented in Appendix B. Here, we only describe the results, in a graphic form. Figure 9 shows the change in the shape of the correlation function of differential conductance fluctuations expected for a spectrometer placed in the center of the bottom surface of a round disk, for various values of the ratio L_c/R, but for the same nominal V_c. This plot shows that the crossover between the quasi-0D (dotted bottom line) and quasi-2D form (solid line) can be split into two steps. First, the negative valley in $K(V)$ at $V \approx V_c$ is reduced (anticorrelations become weaker), which happens without a noticeable change in the width of the correlation function at the half maximum (in units of V/V_c). The following evolution of the form consists of the broadening of the main part of the correlation function. This two-step evolution suggests that the fit to the central peak of the experimentally determined correlation function using the quasi-0D formula is a consistent procedure applicable even across some part of the crossover regime. The need for such a simplified procedure in the following analysis has another reason. When the crossover takes place, the exact form of $K(V)$ becomes dependent on the position of the spectrometer on the surface, that is, its distance to the disk perimeter. This effect is illustrated in the inset to Fig. 9 using several plots of

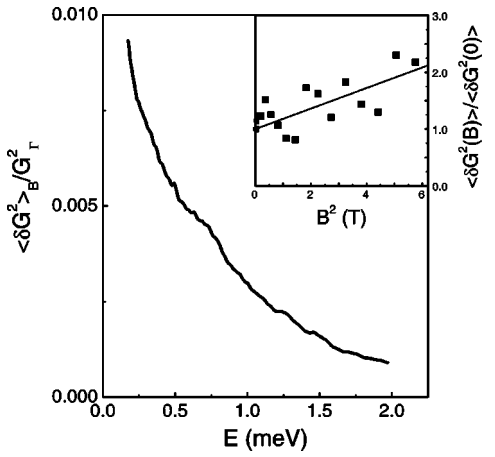

FIG. 10. Inelastic quasiparticle relaxation $\gamma(E)$: Variance of the differential conductance $\delta G(E)^2$ versus excitation energy E. The inset shows the increased variance of fluctuations in classically high magnetic fields $\omega_c\tau\sim 1$.

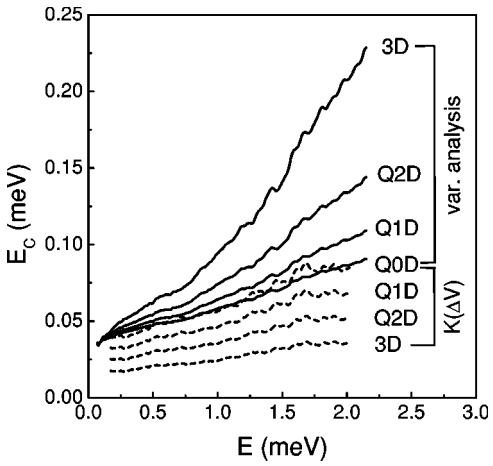

FIG. 11. Comparison of the correlation energy E_c of LDOS fluctuations extracted from the amplitude (solid lines) and the correlation function $K(\Delta V)$ (dashed lines) for different models of quasidimensionality.

$K(\Delta V)$ calculated for different off-center positions of the resonant impurity. Plots in Fig. 9 also show that values of the sum of the physical parameters, $\Gamma+\hbar\gamma$, obtained following such a procedure may be overestimated when the crossover to the quasi-2D limit is more developed.

B. Analysis of the variance of differential conductance fluctuations

Quantitative information about the energy dependence of inelastic quasiparticle relaxation can also be extracted from the bias voltage dependence of the variance of differential conductance fluctuations. Such a dependence for the sample described in this paper is shown in Fig. 10. It is evaluated on the basis of the pattern of raw data in Fig. 4 after subtracting from the data the average conductance, $G(V)$, shown in Fig. 5, then averaging the difference over the magnetic field interval $T<B<1$ T,

$$\mathrm{var}_B G=\frac{1}{1\ \mathrm{T}}\int_{0\ \mathrm{T}}^{1\ \mathrm{T}} dB\,[G(V,B)-\langle G(V)\rangle_B]^2, \qquad (7)$$

and, then smoothing it over the bias voltage interval of 3 times V_c determined for the corresponding bias voltage range in the preceding section. The result is presented in the form normalized by the height of the main conductance peak, G_Γ, in order to exclude from this analysis the parameters of tunneling barriers, and the bias voltage value is converted here into the excitation energy of a quasiparticle (E is the energy of the Fermi sea hole evaluated with respect to the Fermi level). Because of the above-mentioned smoothing procedure, we cannot start the plot in Fig. 10 from exactly $E=0$.

The decrease of the amplitude of differential conductance fluctuations upon the increase of excitation energy of quasiparticles is attributed to a faster inelastic relaxation of the latter, which can be used to study the dependence $\gamma(E)$. Similar to the correlation function, the exact form of such a dependence varies if one makes different assumptions about the effective dimensionality, d:

$$\frac{\langle\delta G^2\rangle}{G_\Gamma^2}=\frac{1}{[1+\hbar\gamma/\Gamma]^{3-d/2}}\times\begin{cases}\dfrac{1/2}{\nu L R^2\Gamma}, & \mathrm{Q0D}\\[2ex] \dfrac{3/16}{\nu R^2\sqrt{\hbar D\Gamma}}, & \mathrm{Q1D}\\[2ex] \dfrac{1/16}{\nu\hbar D L}, & \mathrm{Q2D}\\[2ex] \dfrac{\sqrt{\Gamma/\hbar D}}{32\nu\hbar D}, & \mathrm{3D.}\end{cases} \qquad (8)$$

Using the measured spectrometer width Γ and the known sample dimensions R and L, these equations enable us to obtain theoretical estimates of the amplitude of the variance for a given effective dimensionality. A comparison with the low-E part of the measured variance data plotted in Fig. 10, where we expect $\gamma(E)\sim 0$, shows the best agreement with the Q0D theory. In these estimations we used the value of the mean free path, $l\approx 70$ nm, assigned to the nominal doping level of the buffer layer. This value of l is confirmed by the tendency of the variance $\langle\delta G(B)^2\rangle$ to follow a $[1+(\omega_c\tau)^2]$ dependence[12,8] at classically high magnetic fields $\omega_c\tau\sim 1$ as shown in the inset of Fig. 10.

The energy dependence of the parameter $E_c=\Gamma+\hbar\gamma$ can be extracted from Fig. 10 using the formulas in Eq. (8), and it is plotted in Fig. 11 for the four different effective dimensionalities (upper, solid lines). Also plotted in Fig. 11 is the energy dependence of the parameter $E_c=\alpha V_c$ obtained from the analysis of the correlation function (lower, dashed lines). The values of E_c obtained along two different roots have to coincide for an appropriate dimensionality assumption, and they agree only when analysis is based upon the quasi-0D emitter model.

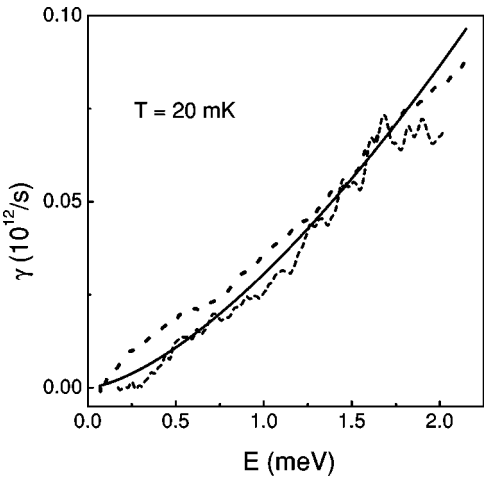

FIG. 12. Determination of the quasiparticle relaxation rate from analysis of correlation (dashed line) and fluctuation data (dotted line). The solid line is a fit to the theoretically expected inelastic particle relaxation rate $\gamma(E)$; see text for details.

C. Quasiparticle inelastic relaxation rate in a disordered conductor

On the basis of the material presented above, we conclude that the use of the quasi-0D assumption for the analysis of fluctuations is fully justified and can be exploited for analyzing the energy dependence of the inelastic relaxation rate of quasiparticles, $\gamma(E)$. The latter can be obtained from the data shown in Fig. 11 by subtracting the original spectrometer width. The resulting relaxation rate dependence on the excitation energy is shown in Fig. 12. This plot contains two sets of data taken from the analysis of correlation functions and the variance, and the comparison to the rate values calculated using Altshuler-Aronov theory. The discrepancy between data worked out in two different ways indicate the arrow bars one would have to assign to the presented analysis.

The theoretical curve shown in Fig. 12 is a fit to the relaxation rate as derived by Sivan, Imry and Aronov,[16] using $E_F=30$ meV for the emitter buffer doped to 4.0×10^{17} cm^{-3} with Si,

$$\gamma=\frac{105\sqrt{3}}{16\pi}\frac{\hbar^{1/2}E^{3/2}}{\tau^{3/2}E_F^2}. \tag{9}$$

The mean free path obtained from this fit is $l=93$ nm, which is close to the mean free path expected for this nominal doping (between $l=50$ nm and $l=100$ nm) and also close to the value extracted from the analysis of the increase of the variance of fluctuations with magnetic field ($l=70$ nm). The use of the three-dimensional expression for the relaxation rate in Eq. (9), in contrast to the quasi-0D model used to describe fluctuations, is justified by the following reason. As discussed at the end of Appendix A, the relaxation of a quasiparticle with energy E is dominated by electron-electron (e-e) collisions with energy transfer comparable to E, and such a rate is determined by correlations between chaotic wave functions with a typical energy separation $\epsilon\approx E$. The latter are formed at the length scale $L_\epsilon\approx\sqrt{\hbar D/\epsilon}$, which has to be compared to the system size: the pillar radius, R, and the width, L. In particular, if $L_\epsilon<L<R$, the e-e interaction can be treated as in the three-dimensional bulk of a disordered conductor. This condition can be expressed more rigorously as $E>\pi^2\hbar D/L^2,\pi^2\hbar D/R^2$, which states that the quasiparticle excitation energy has to be larger than the Thouless energy related to diffusive motion across the pillar. Since the extracted values $\gamma(E)$ sufficiently exceed experimental uncertainty only for quasiparticle excitation energies $E>0.5$ meV (which has to be compared to $\pi^2\hbar D/L^2\approx0.4$ meV), their quantitative comparison to the calculation of $\gamma(E)$ in the 3D limit seems to be consistent. At the same time, the entire interval of energies analyzed in Fig. 12 belongs to a clearly diffusive regime, $E<\hbar\tau\approx4$ meV. Note that of all this analysis is extended only over the low-magnetic-field range, where the Landau quantization of emitter states does not play any role.

IV. SUMMARY

We study resonant tunneling through a discrete localized level in a GaAs/$Al_{1-x}Ga_xAs$ double-barrier heterostructure. The differential conductance exhibits a temperature-insensitive fine structure that is attributed to fluctuations in the local density of states in the doped GaAs emitter. The observed fine structure is analyzed in terms of the variance of the fluctuations in the differential conductance and in terms of correlation functions with respect to voltage. From analyzing the shape of the correlation function we conclude that the effective dimensionality of the emitter is zero and is caused by the disordered interface between the GaAs substrate and the doped buffer layer. In this experiment the electrons tunnel from below the Fermi energy in the heavily doped emitter contact through the discrete localized level, leaving behind a quasihole in the emitter. By quantitatively analyzing the width of the measured correlation functions and the measured variance we are able to extract the energy dependence of the inelastic quasihole relaxation.

ACKNOWLEDGMENTS

We thank A. Förster and H. Lüth for growing the double-barrier heterostructure. We acknowledge financial support from BMBF, DFG, EPSRC, NATO, and TMR.

APPENDIX A:

This appendix presents a qualitative method of estimating the variance of differential conductance fluctuations and the energy dependence of quasiparticle relaxation. It is constructed using a scaling picture similar to that of Thouless[25] by considering what happens to the states of single electrons in a box when the electrons are able to diffuse into other, similar boxes. For clarity we begin by considering three dimensions $d=3$ although this is not necessary for the following arguments to hold. In a classical picture of diffusion, a diffusive path can be viewed as a series of straight line seg-

ments of typical length equal to the elastic mean free path l, where $l=v_F\tau$, τ is the elastic time, and v_F is the Fermi velocity. The classical diffusion coefficient is $D=v_F^2\tau/d$ and the typical time required to diffuse a length ξ is $\tau_D(\xi)=\xi^2/D$.

Consider eight cubes of length ξ that are separated by barriers such that no particles may move between the cubes. We imagine that it is possible to diagonalize the Hamiltonians of the separate cubes and we denote the eigenstates as $\psi_{\alpha i}^{\xi}(r)$ where α specifies the cube and i specifies the state. These states are called ''mother states'' of the generation ξ and they have a mean level spacing $\Delta(\xi)$ where $\Delta(\xi)=1/(\nu\xi^d)$. The states are normalized so that $\int|\psi_{\alpha i}^{\xi}(r)|^2dr=1$. The Hamiltonian of the total system, consisting of eight cubes of size ξ with barriers between them, is also diagonal.

When the barriers between the cubes are removed, particles may diffuse between them. As stated above, the typical time to diffuse a length ξ is $\tau_D(\xi)=\xi^2/D$. The energy corresponding to this time is called the Thouless energy $E(\xi)\approx hD/\xi^2$. Diffusion between cubes produces a finite mixing of states from different Hamiltonians so that the Hamiltonian of the new system (consisting of the eight smaller cubes) is not diagonal. Instead it has finite elements within a distance $E(\xi)$ of the main diagonal and has elements that are approximately equal to zero elsewhere.

An approximation is used to diagonalize the new Hamiltonian. An area of width $E(\xi)$ is centered on the middle of the Hamiltonian and a unitary transformation U is applied to diagonalize it, neglecting the rest of the Hamiltonian. Approximate eigenstates of the new system are linear combinations of a finite number of mother states of the generation ξ,

$$\psi_{\beta n}^{2\xi}(\mathbf{r})\approx\sum_{\alpha i}\ a_{\alpha i}^{\beta n}\psi_{\alpha i}^{\xi}(\mathbf{r}), \tag{A1}$$

where $a_{\alpha i}^{\beta n}$ are coefficients with indices αi that refer to the original cubes of scale ξ and index n of the new states in the cube β of scale 2ξ. The new approximate eigenstates are normalized so that

$$\sum_{n}\ |a_{\alpha i}^{\beta n}|^2\equiv\sum_{\alpha i}\ |a_{\alpha i}^{\beta n}|^2=1, \tag{A2}$$

where we used the property $U^{\dagger}U=1$ (only one value of β is considered). Correlations between local densities remain important because at each level in the scaling procedure there is only a finite basis involved in the construction of new states.

Consider an experimental observation of the local density of states at position $\mathbf{r}_0$. Formally the local density of states may be expressed in terms of a summation of states. When observing through a spectrometer of energy width Γ, then this may be written as a sum of states with energy E_i within Γ of the spectrometer energy E_S,

$$\nu(\mathbf{r}_0;E_S)\approx\Gamma^{-1}\sum_{|E_i-E_S|\leqslant\Gamma}|\psi_{\alpha i}^{\xi}(\mathbf{r}_0)|^2;\quad \xi\leqslant L_\Gamma. \tag{A3}$$

The approximate eigenstates $\psi_{\alpha i}^{\xi}(\mathbf{r}_0)$ are those in a system of size ξ, where $\xi\leqslant L_\Gamma$ and L_Γ is the length scale corresponding to energy Γ, $L_\Gamma\approx\sqrt{hD/\Gamma}$. In general, however, the system is larger than L_Γ and it is necessary to know how the summation above behaves at larger scales $\xi>L_\Gamma$. Consider, for example, a system of scale $\xi=2L_\Gamma$. Applying the scaling procedure above we may write the approximate eigenstates at larger scales using Eq. (A1), giving

$$\begin{aligned}\nu(\mathbf{r}_0;E_S)&\approx\Gamma^{-1}\sum_{|E_i-E_S|\leqslant\Gamma}|\psi_{\alpha i}^{\xi=2L_\Gamma}(\mathbf{r}_0)|^2\\&\approx\Gamma^{-1}\sum_{n}\ \sum_{\alpha i}\ |a_{\alpha i}^{\beta n}|^2|\psi_{\alpha i}^{L_\Gamma}(\mathbf{r}_0)|^2\\&\approx\Gamma^{-1}\sum_{\alpha i}\ |\psi_{\alpha i}^{L_\Gamma}(\mathbf{r}_0)|^2,\end{aligned} \tag{A4}$$

where in the last step we used the normalization condition given in Eq. (A2). This result shows that the summation over the energy interval Γ will not vary when the spectrum is modified into its final form at the total system size L, but it will depend on the spectrum at length scale L_Γ. This is because once the scale $\xi>L_\Gamma$, then the corresponding energy $E(\xi)<\Gamma$ and information about correlations that is carried by the mother states will remain in the energy interval Γ no matter how large ξ becomes. Now we describe the application of the scaling picture above to the differential conductance.[12,8] The current in the plateau regime, I, is determined by a sum of local densities of the wave functions $|\psi_E(\mathbf{r})|^2$ with energy, E, taken in an energy interval Γ around the energy E_0, $I\propto\nu\sim\Gamma^{-1}\Sigma|\psi_E(\mathbf{r})|^2$. The number of states in a sample of volume L^d within the energy interval Γ is $N(\Gamma,L)\approx\nu_0\Gamma L^d$, where ν_0 is the mean density of states per unit volume, per unit energy. The variance of the differential conductance, $\langle\delta G^2\rangle$, is given by a typical fluctuation in the density of states $\delta\nu$ divided by the typical energy interval Γ. As described above, a summation over the energy interval Γ depends on the spectrum at length scale L_Γ with number of states $N(\Gamma,L_\Gamma)$.[12,8] Since $\psi_E(\mathbf{r})$ from a single state is a random variable with mainly Gaussian statistics in the metallic regime[22] and the variance, $\langle\delta G^2\rangle$, is given by a sum of the individual variances, we have

$$\langle\delta G^2\rangle\sim\frac{N(\Gamma,L_\Gamma)\langle|\psi_E(\mathbf{r})|^2\rangle^2}{\Gamma^2V_\Gamma^2},$$

where the typical density of a single state is $\langle|\psi_E(\mathbf{r})|^2\rangle\sim1/L_\Gamma^d$.

In the estimation above V_Γ is the smallest voltage step that is given by the spectrometer width $V_\Gamma\sim\Gamma/e$. An additional level broadening, $\hbar\gamma$, takes into account relaxation processes in the bulk of the emitter and results in a total level broadening $\Gamma(1+\hbar\gamma/\Gamma)$. Counting powers of Γ in the estimation of $\langle\delta G^2\rangle$ at the end of the preceding paragraph leads to a factor of $(1+\hbar\gamma/\Gamma)^{d/2-3}$ in the variance. However, we should stress that the level broadening $\hbar\gamma$ does not influence the average value of the current in the plateau regime,

$$\langle I\rangle\sim\frac{N(\Gamma,L_\Gamma)\langle|\psi_E(\mathbf{r})|^2\rangle}{\Gamma},$$

or the height of the main differential peak, which is given by the mean current divided by the width of the peak,

$$G_\Gamma \sim \frac{N(\Gamma,L_\Gamma)\langle|\psi_E(\mathbf{r})|^2\rangle}{\Gamma V_\Gamma}.$$

Thus the variance is parametrically reduced as compared to G_Γ^2 by a factor $1/N(\Gamma,L_\Gamma)$, where $N(\Gamma,L_\Gamma)\sim g(L_\Gamma) \sim \nu D^{d/2}\Gamma^{1-d/2}$. When the dimension d refers to the effective dimensionality of the system as determined by the volume over which mesoscopic fluctuations occur, embedded in a nominally three-dimensional space, then the factor $N(\Gamma,L_\Gamma)$ is replaced by $N(\Gamma,L_\Gamma)L^{3-d}$. In this case the variance may be written as

$$\langle \delta G^2\rangle \sim \frac{1}{\nu D^{d/2}\Gamma^{1-d/2}L^{3-d}} \frac{G_\Gamma^2}{(1+\hbar\gamma/\Gamma)^{3-d/2}}.$$

It is also possible to explain the energy dependence of the inelastic scattering rate in terms of the above scaling picture. The rate is determined by a collision between four particles involving transferred energy ω. There are two initial particles with energies $E>0$ and $\epsilon'<0$ and two final particles with energies $E-\omega>0$ and $\epsilon'+\omega>0$. The inelastic rate may be estimated using Fermi's golden rule:[16,31–33]

$$\gamma(\xi)\sim \sum_{0<\omega<E} \sum_{-\omega<\epsilon'<0} \frac{|M(E,\epsilon',\omega)|^2}{\Delta(\xi)},$$

where $M(E,\epsilon',\omega)$ is the matrix element for the collision. For a short-ranged interaction the matrix elements are given by a spatial integration of a product of four single-particle wave functions[31,32]

$$\frac{M(E,\epsilon',\omega)}{\Delta(\xi)} \approx \xi^d \int d^d r\, \psi^*_{\epsilon'+\omega}(\mathbf{r})\psi^*_{E-\omega}(\mathbf{r})\psi_{\epsilon'}(\mathbf{r})\psi_E(\mathbf{r}).$$

The normalized wave functions in a disordered system exhibit random spatial oscillations, each typically contributing $|\psi|^2\sim\xi^{-d}$. After disorder and spatial averaging the product of four wave functions is roughly

$$\langle \psi^4\rangle \sim \frac{1}{\xi^{2d}N(E(\xi),\xi)}.$$

In the limit $N(E(\xi),\xi)\to\infty$, there is an infinite basis involved in the construction of new states at each level of the scaling process, leading to an absence of correlations between different eigenvectors. For finite $N(E(\xi),\xi)$, however, there is a finite basis and correlations exist. Integration over the hypercube provides an additional factor of ξ^d so that a typical value of the matrix element is

$$M\sim \frac{\Delta(\xi)}{N(E(\xi),\xi)}.$$

Since each summation with respect to energy contributes roughly $E/\Delta(\xi)$, we find

$$\gamma(\xi)\sim \frac{E^2}{N^2(E(\xi),\xi)\Delta(\xi)}.$$

Now we consider what occurs when the hypercubes are scaled up to the total system size L. For small energies, $E<E(L)\equiv E_{\mathrm{Th}}$, the system is in the zero-dimensional limit whereby the system size is always less than the length scale associated with the energy, L_E, where $L_E\approx\sqrt{hD/E}$. The above estimation holds for all scales up to the system size so that the inelastic rate is[16,33] $\gamma\sim E^2/[g^2(L)\Delta(L)]$, where $g(L)\sim N(E_{\mathrm{Th}},L)$. For our case of interest, however, we sum over states up to energies greater than the Thouless energy E_{Th} of the total system, $E>E(L)\equiv E_{\mathrm{Th}}$. When the system size reaches L_E, the energy scale E contains all the information about correlations between the states. As for the calculation of $\langle\delta G^2\rangle$ at the length scale L_Γ, further scaling does not change the evaluation of the relaxation rate. The summation over the energy interval E will not vary when the spectrum is modified into its final form at the total system size L, but it will depend on the spectrum at length scale L_E with number of states $N(E,L_E)$. We replace ξ in the above estimation with L_E, giving

$$\gamma(E)\sim \frac{E^2}{N^2(E,L_E)\Delta(L_E)}\sim \frac{E^{3/2}}{E_F^2\tau^{3/2}},$$

in agreement with the prediction of Altshuler and Aronov.[15]

APPENDIX B:

This appendix describes a numerical calculation of the correlation function in a disk of width L and radius R where $L\ll R$. The crossover regime between the quasi-0D ($L\ll R\ll L_c$) and quasi-2D ($L\ll L_c\ll R$) limits is studied. Using standard diagrammatic perturbation theory techniques, it is possible to express the correlation function in terms of diffusion propagators in the disk.[12] Since $L\ll L_c$, the zero mode dominates the diffusion propagator in the direction parallel to the current flow, across the width of the disk, but it is necessary to sum all harmonics of diffusion perpendicular to the current flow, in the plane of the disk. Adopting circular cylindrical coordinates $\mathbf{r}=(\rho,\phi,z)$, we consider the resonant impurity to be positioned at one side of the disk $z=0$ and at an arbitrary radius $0\leqslant\rho\leqslant R$ from the center of the disk.

The numerical procedure outlined here is necessary only in the crossover regime since the exact geometry of the emitter is not relevant in the limiting cases: in the quasi-2D limit a diffusing electron typically does not reach the boundary of the disk and it is thus possible to integrate over all harmonics of the diffusion propagator in the plane of the disk, whereas in the quasi-0D limit the zero mode in the plane of the disk is not damped very effectively and it dominates, enabling one to neglect all higher harmonics. These approximations produce the analytic results given in the main text and in both cases the position of the resonant impurity ρ is irrelevant. However, the position of the resonant impurity is crucial in the crossover regime because it is necessary to sum

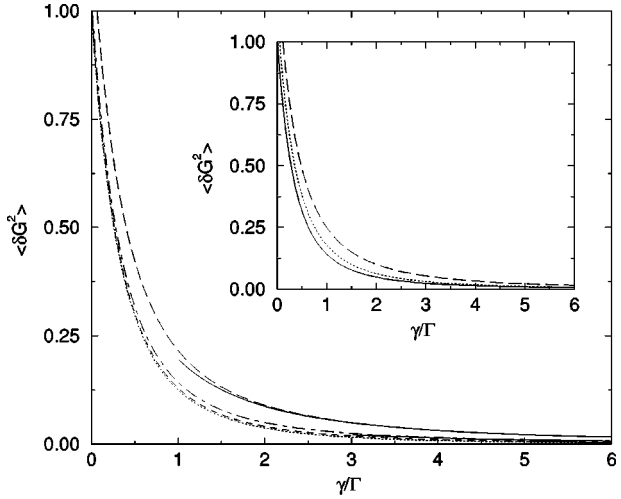

FIG. 13. Theoretical form of the variance $\langle \delta G^2 \rangle$ as a function of $\hbar\gamma/\Gamma$ with the resonant impurity in the center of the disk $\rho/R=0$. From the top, the long dashed line is the numerical result for $L_\Gamma/R=1.0$, dot-dashed line for $L_\Gamma/R=1.5$, and short dashed line for $L_\Gamma/R=2.0$. The solid lines show asymptotics at large $\hbar\gamma/\Gamma$ given by the Q2D analytic result, Eq. (8), and the dotted line is the Q0D analytic result, Eq. (8). All the curves are normalized by the Q0D analytic result, Eq. (8). Inset is $\langle \delta G^2 \rangle$ as a function of $\hbar\gamma/\Gamma$ for $L_\Gamma/R=1.5$ and different impurity positions. Solid line is $\rho/R=0$, dotted line is $\rho/R=0.5$, and long dashed line is $\rho/R=1.0$.

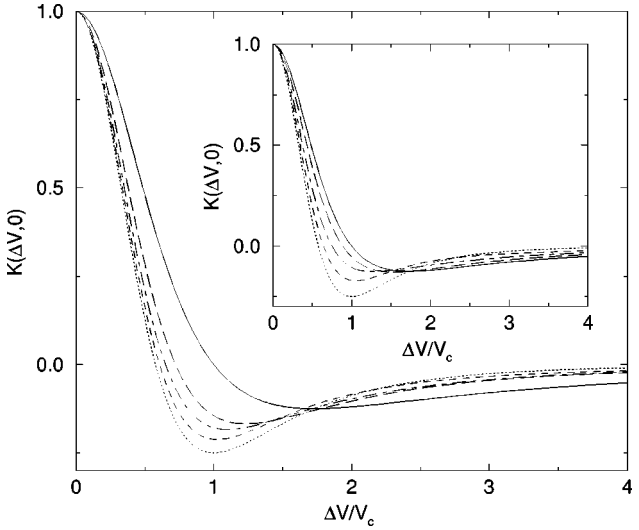

FIG. 14. Theoretical form of the correlation function $K(\Delta V,0)$ as a function of $\Delta V/V_c$ with the resonant impurity off center of the disk at $\rho/R=0.5$. The long dashed line is the numerical result for $L_c/R=1.0$, dot-dashed line for $L_c/R=1.5$, and short dashed line for $L_c/R=2.0$. Solid and dotted lines are the Q2D and Q0D analytic results from Eq. (4). Inset is $K(\Delta V,0)$ as a function of $\Delta V/V_c$ with the resonant impurity at $\rho/R=1.0$ with line styles the same as the main part.

over many harmonics that are influenced by the exact geometry of the emitter.

The correlation function of differential conductances can be obtained from the disordered averaged current-current correlation function[13] $\langle \delta I(V)\delta I(V')\rangle$ by taking the second derivative with respect to $\Delta=\alpha e(V-V')$,

$$\langle \delta G(V)\delta G(V')\rangle = -(\alpha e)^2 \frac{\partial^2}{\partial \Delta^2}\langle \delta I(V)\delta I(V')\rangle.$$

By expressing the current in terms of Green's functions using the single-particle Breit-Wigner resonance conductance formula,[27–29,18] the correlation function takes the form[12]

$$\langle \delta G(V)\delta G(V')\rangle = -\frac{1}{\beta}\left(\frac{G_\Gamma \Gamma}{2}\right)^2\left(\frac{\partial^2}{\partial\Delta^2}\right)\frac{\Gamma}{\nu}\int \frac{d\omega[P_\omega(\mathbf{r},\mathbf{r})+P_{-\omega}(\mathbf{r},\mathbf{r})]}{(\hbar\omega-\Delta)^2+\Gamma^2}. \tag{B1}$$

In the absence of time-reversal symmetry, the variance changes only by the standard Dyson's factor of $1/\beta$, where $\beta=1$ for the orthogonal ensemble (in the presence of impurity scattering only) and $\beta=2$ for the unitary ensemble (in the presence of a finite magnetic field or weak scattering by magnetic impurities that breaks time-reversal invariance). The diffusion propagator in the disk, $P_\omega(\mathbf{r},\mathbf{r})$, satisfies the following equation

$$[-D\nabla^2+\gamma-i\omega]P_\omega(\mathbf{r},\mathbf{r}')=\delta(\mathbf{r}-\mathbf{r}'). \tag{B2}$$

It describes diffusion in the disk and is therefore restricted by the tunneling barrier at $z=0$ and an insulating boundary at the cylinder surface $\rho=R$. The poorly conducting interface between the emitter and substrate is also modeled as a tunneling barrier at $z=L$. These boundary conditions are expressed as

$$\partial_z P|_{z=0}=0, \quad \partial_\rho P|_{\rho=R}=0, \quad \partial_z P|_{z=L}=0. \tag{B3}$$

The correlation function is found by solving the diffusion equation, Eq. (B2), in the presence of the boundary conditions, Eq. (B3). The angle ϕ is set to zero without loss of generality and we find

$$P_\omega(\mathbf{r},\mathbf{r})=\frac{1}{\pi R^2 L}\sum_{m,\alpha_{nm}}\frac{J_m^2(\alpha_{nm}\rho/R)}{(1-m^2/\alpha_{nm}^2)J_m^2(\alpha_{nm})} \times\frac{1}{(D\alpha_{nm}^2/R^2+\gamma-i\omega)}, \tag{B4}$$

where $m=0,\pm1,\pm2,\ldots$ and J_m is a Bessel function of the first kind of order m. For a given m, the numbers α_{nm} are solutions of the boundary condition at the cylinder surface $\rho=R$,

$$\partial_\rho J_m(\alpha_{nm}\rho/R)|_{\rho=R}=0,$$

which may be expressed as

$$mJ_m(\alpha_{nm})=\alpha_{nm}J_{m+1}(\alpha_{nm}).$$

We solve this boundary condition numerically in order to calculate the propagator, giving the variance and the correlation function for arbitrary L_c/R and $0\leqslant\rho\leqslant R$.

In the main text Fig. 9 shows the correlation function for different L_c/R and $\rho/R=0$ (main part) and for different impurity positions ρ/R (inset). We present here for completeness some further numerical results. Figure 13 shows the calculated variance $\langle \delta G^2 \rangle$ as a function of $\hbar\gamma/\Gamma$ with the resonant impurity at the center of the disk $\rho/R=0$ and different values of L_Γ/R. The short dashed line is the Q0D analytic result, Eq. (8), whereas the solid lines show asymptotics at large $\hbar\gamma/\Gamma$ given by the Q2D analytic result, Eq. (8). As expected, the numerical plots show behavior similar to the Q0D analytic form for $L_c \gg R$ (small $\hbar\gamma/\Gamma$) and similar to Q2D for $L_c \ll R$ (large $\hbar\gamma/\Gamma$) with a crossover at $L_c \approx R$. To analyze the effect of the position of the impurity we choose a particular value of L_Γ/R. The inset of Fig. 13 is $\langle \delta G^2 \rangle$ for $L_\Gamma/R=1.5$ and for different impurity positions. When the impurity position is off-center the variance has a similar qualitative form as for the impurity on the cylinder axis, but the fluctuations appear to be generally larger.

Figure 14 shows $K(\Delta V,0)$ as a function of $\Delta V/V_c$ and different values of L_c/R for $\rho/R=0.5$ (main part) and $\rho/R=1.0$ (inset). The crossover appears to occur more slowly (over a larger range of L_c/R) when the impurity position is off-center.

[1] B. Su, V. J. Goldman, and J. E. Cunningham, Phys. Rev. B **46**, 7644 (1992).

[2] M. W. Dellow, P. H. Beton, C. J. G. M. Langerak, T. J. Foster, P. C. Main, L. Eaves, M. Henini, S. P. Beaumont, C. D. W. Wilkison, Phys. Rev. Lett. **68**, 1754 (1992); A. K. Geim, P. C. Main, N. Jr. La Scala, L. Eaves, T. J. Foster, P. H. Beton, J. W. Sakai, F. W. Sheard, M. Henini, G. Hill, and M. A. Pate, Phys. Rev. Lett. **72**, 2061 (1994); P. J. McDonnell, A. K. Geim, P. C. Main, T. J. Foster, P. H. Beton, and L. Eaves, Physica B **211**, 433 (1995).

[3] M. Tewordt, L. Martin-Moreno-L, V. J. Law, M. J. Kelly, R. Newbury, M. Pepper, D. A. Ritchie, J. E. F. Frost, and G. A. C. Jones, Phys. Rev. B **46**, 3948 (1992); M. Tewordt, L. Martin-Moreno, J. T. Nicholls, M. Pepper, M. J. Kelly, V. J. Law, D. A. Ritchie, J. E. F. Frost, and G. A. C. Jones, *ibid.* **45**, 14407 (1992); T. Schmidt, M. Tewordt, R. H. Blick, R. J. Haug, D. Pfannkuche, K. v. Klitzing, A. Förster, and H. T. Lüth, *ibid.* **51**, 5570 (1995).

[4] M. R. Deshpande, J. W. Sleight, M. A. Reed, R. G. Wheeler, and R. J. Matyi, Phys. Rev. Lett. **76**, 1328 (1996); J. W. Sleight, E. S. Hornbeck, M. R. Deshpande, R. G. Wheeler, M. A. Reed, R. C. Bowen, W. R. Frensley, J. N. Randall, and R. J. Matyl, Phys. Rev. B **53**, 15 727 (1996).

[5] T. Schmidt, R. J. Haug, V. I. Fal'ko, K. v. Klitzing, A. Förster, and H. Lüth, Europhys. Lett. **36**, 61 (1996).

[6] T. Schmidt, R. J. Haug, V. I. Fal'ko, K. v. Klitzing, A. Förster, and H. Lüth, Phys. Rev. Lett. **78**, 1540 (1997).

[7] P. C. Main, A. S. G. Thornton, R. J. A. Hill, S. T. Stoddart, T. Ihn, L. Eaves, K. A. Benedict, and M. Henini, Phys. Rev. Lett. **84**, 729 (2000).

[8] J. P. Holder, A. K. Savchenko, V. I. Fal'ko, B. Joualt, G. Faini, F. Laruelle, and E. Bedel, Phys. Rev. Lett. **84**, 1563 (2000).

[9] P. König, T. Schmidt, and R. J. Haug, cond-mat/0004165 (unpublished).

[10] T. Schmidt, P. König, E. McCann, V. I. Fal'ko, and R. J. Haug, Phys. Rev. Lett. **86**, 276 (2001).

[11] U. Sivan, F. P. Milliken, K. Milkove, S. Rishton, Y. Lee, J. M. Hong, V. Boegli, D. Kern, and M. Defranza, Europhys. Lett. **25**, 605 (1994).

[12] V. I. Fal'ko, Phys. Rev. B **56**, 1049 (1997).

[13] I. V. Lerner, Phys. Lett. A **133**, 253 (1988).

[14] The quasiparticle to be considered below is, in fact, a nonequilibrium hole left after the tunneling process below the Fermi level in the emitter. Relaxation of higher-energy electrons into this emptied state results in a finite lifetime of such hole.

[15] B. L. Altshuler and A. G. Aronov, Pis'ma Zh. Éksp. Teor. Fiz. **30**, 514 (1979) [JETP Lett. **30**, 482 (1979)]; Solid State Commun. **38**, 11 (1981); B. L. Altshuler and A. G. Aronov, in *Electron-Electron Interactions in Disordered Systems*, edited by A. L. Efros and M. Pollack (North-Holland, Amsterdam, 1985).

[16] U. Sivan, Y. Imry, and A. G. Aronov, Europhys. Lett. **28**, 115 (1994).

[17] L. I. Glazman and K. A. Matveev, Pis'ma Zh. Éksp. Teor. Fiz. **48**, 403 (1988) [JETP Lett. **48**, 445 (1988)]; L.Y. Chen, and C.S. Ting, Phys. Rev. B **44**, 5916 (1991).

[18] I. V. Lerner, M. E. Raikh, Phys. Rev. B **45**, 14 036 (1992).

[19] B. L. Altshuler and D. E. Khmelnitskii, Pis'ma Zh. Éksp. Teor. Fiz. **42**, 294 (1985) [JETP Lett. **42**, 359 (1985)].

[20] A. I. Larkin and D. E. Khmelnitskii, Zh. Éksp. Teor. Fiz. **91**, 1815 (1987) [Sov. Phys. JETP **64**, 1075 (1987)].

[21] V. I. Fal'ko and D. E. Khmelnitskii, Zh. Éksp. Teor. Fiz. **95**, 349 (1989) [Sov. Phys. JETP **68**, 186 (1989)].

[22] V. I. Fal'ko and K. B. Efetov, J. Math. Phys. **37**, 4935 (1996).

[23] K. B. Efetov, Adv. Phys. **32**, 53 (1983).

[24] V. I. Fal'ko and K. B. Efetov, Phys. Rev. B **50**, 11 267 (1994).

[25] D. J. Thouless, Phys. Rev. Lett. **39**, 1167 (1977).

[26] M. Tewordt, V. J. Law, M. J. Kelly, R. Newbury, M. Pepper, D. C. Peacock, J. E. F. Frost, D. A. Ritchie, and G. A. C. Jones, J. Phys.: Condens. Matter **2**, 8969 (1990).

[27] A. Chaplik and M. Entin, Zh. Éksp. Teor. Fiz. **67**, 208 (1974) [Sov. Phys. JETP **40**, 106 (1974)].

[28] M. Azbel, Solid State Commun. **45**, 527 (1983).

[29] W. Xue and P. A. Lee, Phys. Rev. Lett. **38**, 3913 (1988).

[30] For a while, we forget about the electron spin, but the final result will be written in such a form that this flaw will be automatically corrected—if there is no spin-orbit scattering in the bulk. Otherwise, the parameter β in the answers should be taken as $\beta=2$.

[31] Ya. M. Blanter, Phys. Rev. B **54**, 12 807 (1996).

[32] B. L. Altshuler, Y. Gefen, A. Kamenev, and L. S. Levitov, Phys. Rev. Lett. **78**, 2803 (1997).

[33] B. L. Altshuler, M. E. Gershenson, and I. L. Aleiner, Physica E **3**, 58 (1998); I. L. Aleiner, B. L. Altshuler, and M. E. Gershenson, Waves Random Media **9**, 201 (1999).